Open access • Journal Article • DOI:10.1086/187206

A measurement of the medium-scale anisotropy in the cosmic microwave background radiation — Source link

Edward Cheng, D. A. Cottingham, D. J. Fixsen, C. A. Inman ...+5 more authors

Institutions: Goddard Space Flight Center, Massachusetts Institute of Technology, Princeton University

Published on: 20 Feb 1994 - The Astrophysical Journal (IOP Publishing Ltd.)

Topics: Cosmic microwave background

A Measurement of the Medium-Scale Anisotropy in the Cosmic Microwave Background Radiation

E. S. Cheng[1], D. A. Cottingham[2], D. J. Fixsen[3], C. A. Inman[4], M. S. Kowitt[1], S. S. Meyer[4], L. A. Page[5], J. L. Puchalla[4], and R. F. Silverberg[1]

Received ______________________; accepted ______________________

Submitted to *Ap. J. Letters* 18 May 1993, Revised 9 Nov 1993

[1]NASA/Goddard Space Flight Center, Code 685.0, Greenbelt, MD 20771

[2]Global Science and Technology, Inc., NASA/GSFC Code 685.0, Greenbelt, MD 20771

[3]Applied Research Corporation, NASA/GSFC Code 685.3, Greenbelt, MD 20771

[4]Massachusetts Institute of Technology, Room 20B-145, Cambridge, MA 02139

[5]Princeton University Physics Dept., Princeton, NJ 08544

ABSTRACT

Observations from the first flight of the Medium Scale Anisotropy Measurement (MSAM) are analyzed to place limits on Gaussian fluctuations in the Cosmic Microwave Background Radiation (CMBR). This instrument chops a $30'$ beam in a 3 position pattern with a throw of $\pm 40'$; the resulting data is analyzed in statistically independent single and double difference datasets. We observe in four spectral channels at 5.6, 9.0, 16.5, and 22.5 cm^{-1}, allowing the separation of interstellar dust emission from CMBR fluctuations. The dust component is correlated with the *IRAS* 100 μm map. The CMBR component has two regions where the signature of an unresolved source is seen. Rejecting these two source regions, we obtain a detection of fluctuations which match CMBR in our spectral bands of $0.6 \times 10^{-5} < \Delta T/T < 2.2 \times 10^{-5}$ (90% CL interval) for total rms Gaussian fluctuations with correlation angle $0\overset{\circ}{.}5$, using the single difference demodulation. For the double difference demodulation, the result is $1.1 \times 10^{-5} < \Delta T/T < 3.1 \times 10^{-5}$ (90% CL interval) at a correlation angle of $0\overset{\circ}{.}3$.

Subject headings: cosmology: cosmic microwave background — cosmology: observations

1. Introduction

Measurements of the anisotropy of the Cosmic Microwave Background Radiation (CMBR) on $0.^{\circ}5$ angular scales have received greater attention (Efstathiou *et al.*, 1992, Gorski 1993, Kashlinsky 1992) after the *COBE* detection on large angular scales (Smoot *et al.* 1992). The large-scale measurement sets an amplitude for the unperturbed primeval density fluctuation spectrum; at scales between $0.^{\circ}5$ and 2°, the anisotropy could be enhanced through Doppler and heating effects. The first flight of the Medium Scale Anisotropy Measurement (MSAM) has led to a detection of brightness fluctuations at $0.^{\circ}5$ which are consistent with a CMBR spectral signature. The instrument, observations, analysis, and results are described below.

2. Instrument Description

MSAM is a balloon-borne 30° off-axis Cassegrain telescope consisting of a 1.4 m aluminum primary, a 0.27 m nutating secondary, and a four channel radiometer previously flown in the Far Infra-Red Survey experiment (Page 1989, Page *et al.* 1990, Meyer *et al.* 1991). The beam size of the telescope is $30'$. The secondary executes a 2 Hz, four-position, square-wave chop (*i.e.* center, left, center, right) with an amplitude of $\pm 40'$ on the sky. Each position consists of a 23 ms transition and a 102 ms stable integration where the RMS position jitter is less than $4''$. The bolometric detectors have bandpass central frequencies of 5.6, 9.0, 16.5, and 22.5 cm^{-1} each with ~ 1 cm^{-1} bandwidth (Page *et al.* 1993). The bolometer output is sampled synchronously at 32 Hz with an integrating A/D converter.

The telescope is shielded with aluminized panels so that the dewar horn, the secondary and the geometrically illuminated portion of the primary have no view of the Earth or the lower part of the flight train. The edge of the balloon, as seen by the telescope, extends about 25° from the zenith. Ground-based measurements of the sidelobe pattern show the response to the ground to be less than -60 dB of the central lobe of the antenna pattern.

3. Observations

The package was launched from Palestine, Texas at 0059 UT 5 June 1992, and reached float altitude of 38 km at 0507 UT. The flight ended with sunrise on the package at

1056 UT. During the flight, we scanned Jupiter and Saturn to calibrate the instrument and to map the antenna pattern, scanned over the center of the Coma cluster to search for the Sunyaev-Zel'dovich effect (which will be reported in a future *Letter*), and integrated for 4.9 hours on a patch of sky near the north celestial pole to search for CMBR anisotropy.

The CMBR observations are made by looking 8° above the north celestial pole, and holding elevation constant while scanning in azimuth $\pm 45'$ with a period of 1 minute. We start with the center of the scan $21'$ to the east of the meridian and track for 20 minutes; at this point the center of the scan is $21'$ to the west of the meridian. We then pause for about 40 s to record an image with the star camera and correct for gyro drift, and begin a new 20 minute scan $42'$ to the east of the previous scan. Thus, half of each 20 minute scan overlaps the following scan. This observation strategy minimizes motion of the telescope relative to the Earth and the atmosphere, and therefore also minimizes any systematic contribution from these sources. We completed 6 scans from 0419 to 0622 UT, observed the Coma cluster for 40 minutes, and completed an additional 8 scans from 0701 to 0950 UT, for a total of 14 scans. This covers two strips at declination $82\overset{\circ}{.}0$, from right ascension $14\overset{h}{.}44$ to $16\overset{h}{.}89$, and from $17\overset{h}{.}18$ to $20\overset{h}{.}33$ (J1992.5). We refer to these two segments as the two halves of the flight.

4. Data Analysis

4.1. Calibration, Deglitching, and Demodulation

The instrument is calibrated by in-flight observations of Jupiter before the CMBR scans, and of Saturn after the CMBR scans. We use Jupiter as our definitive calibration, with Saturn as a comparison. For the night of observation the apparent diameter of Jupiter is $35''$, and the diameter of the disk of Saturn is $17\overset{''}{.}6$. We take the spectrum of Jupiter from Griffin *et al.* 1986, from which we derive antenna temperatures for our four channels of 172, 170, 148, and 148 K respectively. We assume that in our spectral region Saturn has a Rayleigh-Jeans spectrum with a temperature of 133 ± 20 K (Harwit 1988, Lang 1980). No correction is made for the rings of Saturn, which at this frequency add less than 10% in brightness (Hanel *et al.* 1981). The calibrations on Jupiter and Saturn are consistent in channels 1, 3, and 4. In channel 2, Saturn is dimmer than we expected by a factor of two. In addition, the offset in channel 2 drifts downward by the same factor over the same period, and the noise also follows this drift. We assume that a post-detection gain drift is responsible for this behavior, and we correct this by multiplying the channel 2 data by a linear function of time to make the Jupiter and Saturn calibrations consistent. With this correction, the offset stability in channel 2 becomes consistent with that of the other channels. The uncertainty in the calibration is 10% (Griffin *et al.* 1986).

The data contain large spikes, or glitches, at a rate of once per 2 to 5 s, consistent with cosmic rays striking the detectors (Charakhch'yan *et al.* 1978). To remove these glitches, we perform a first cut at $10\,\sigma$, and then deconvolve with a model of the transfer function of the detectors. The average offset signal in a chop cycle for each half of the flight is then subtracted from all chop cycles in that half, after which two cuts at $3.5\,\sigma$ are made. About 5% of the data is cut this way.

We estimate instrument noise by forming the autocorrelation of the deglitched data, filtering out 0 Hz and harmonics of 2 Hz, where sky signals appear. This estimate is therefore unaffected by any optical signal. We form this estimate for each 20 minute segment of data which is then propagated through the remaining processing. All χ^2 reported below are with regard to these error bars.

The data are demodulated in two different ways. The first corresponds to summing the periods when the secondary is in the central position, and subtracting the periods when it is to either side; we call this the double-difference demodulation. This demodulation is insensitive to atmospheric gradients. The second demodulation corresponds to differencing the periods when the secondary is to the right from those when it is to the left, and ignoring the periods when the secondary is in the center; we call this the single-difference demodulation. These two demodulations of the data yield statistically independent measurements of the sky. We use the scan over Jupiter to deduce an optimal demodulation of the infrared signal. Each group of four complete chopper cycles (2 s) is averaged together to form a "record." Records for which there are too few samples to form a robust average, due to deglitching or telemetry dropouts, are deleted. The procedure results in a 2% data loss. Each record is then demodulated to produce one single and one double difference observation every 2 s.

This demodulated signal has had a constant offset removed from it in the deglitching process. The size of this offset is approximately 10 mK Rayleigh-Jeans in all four bands, and in both the single and double difference demodulation. To remove the drift in this offset, we subtract a slowly varying function of time to minimize the variance of observations of each point in the sky made at different times. The function of time is implemented as a cubic spline with a knot every 2.5 minutes. Each channel and demodulation is treated separately. The two halves of the flight are also treated separately, as they are separated in time and do not overlap on the sky. The drift is $\lesssim 400\mu$K Rayleigh-Jeans, and significant at the 3–$8\,\sigma$ level; thus the offset is constant to about 4%. The reduced χ^2 of these fits range from 0.92

to 1.21.

The data are binned by position on the sky, and by relative angular orientation of the antenna beam with respect to the local tangent to the circle of constant declination at the central beam location. The bin size is $0\overset{\circ}{.}12$ in position, and 10° in angular orientation. Records which differ from the median in the bin by more than $3\,\sigma$ are deleted. Following this, bins containing fewer than 10 records are deleted. The reduced χ^2 of the binned data after removing a mean from each bin ranges from 0.88 to 1.04 for the various channels and demodulations, indicating that our observations of the sky are consistent. The binned data contains 86% of all the data originally taken, with an achieved sensitivity in each of the four channels of 400, 210, 140, and 330 μK $\sqrt{\rm s}$ Rayleigh-Jeans. For channels 1 and 2 this is 810 and 1190 μK $\sqrt{\rm s}$ CMBR.

4.2. Spectral Model of the Sky

To extract the part of the signal due to variations in the CMBR, we fit the data t_{ck} for each channel c and sky bin k to a two component model:

$$t_{ck} = \int d\nu\, F_c(\nu) \left[D_k \left(\frac{\nu}{\nu_0}\right)^{\alpha} B_\nu(T_{\rm D}) + t_k \left.\frac{dB_\nu}{dT}\right|_{T_{\rm CMBR}} \right], \tag{1}$$

where $F_c(\nu)$ is the spectral response of the instrument, $B_\nu(T)$ is the Planck function at temperature T, $T_{\rm D} = 20\,{\rm K}$ is the dust temperature, $\alpha = 1.5$ is the spectral index of the dust, $\nu_0 = 22.5$ cm^{-1} is the reference frequency, $T_{\rm CMBR} = 2.73\,{\rm K}$ is the temperature of the CMBR, and D_k and t_k are free parameters. The result is a component sensitive to the CMBR (t_k) and a component sensitive to the dust (D_k). The χ^2 for the fit is 237/292 for the single difference data, and 454/294 for the double differenced data. $T_{\rm D}$ and α are fixed for this analysis since varying these parameters by reasonable amounts does not significantly change the CMBR component. Fig. 1 shows the dust channel. The superimposed curve is an approximation of the expected dust emission produced by convolving our antenna pattern with IRAS 100 μm measurements (Wheelock *et al.* 1991, Wheelock *et al.* 1993). For the most part agreement is quite good, but in a few places they differ quite significantly. The scaling of the *IRAS* data is determined by fitting to the dust channel; this scaling is equivalent to an average spectral index between 100 μm and 444 μm (22.5 cm^{-1}) of 1.5 ± 0.2. Fig. 2 shows the CMBR component. For clarity, these plots are binned more coarsely than the data we analyzed, and do not distinguish between points taken at slightly different declination or antenna orientation.

There are two candidate unresolved sources visible in the CMBR spectral component, ΔT_k, for both the single and double difference data. The more prominent source (MSAM 15+82) is located at RA $14^{\rm h}\!.92 \pm 0^{\rm h}\!.03$ in a dust-free region, and has a measured flux density of 4.5 ± 0.7 Jy at 5.6 cm^{-1} (error bar includes calibration uncertainty of 10%). The second, dimmer, candidate (MSAM 19+82) is located at RA $19^{\rm h}\!.29 \pm 0^{\rm h}\!.03$, and has a measured flux density of 3.6 ± 0.6 Jy at 5.6 cm^{-1}. It is in a region that is somewhat confused by foreground dust emission. We observe at a fixed declination so the declination coordinate for these sources is less well determined, but it is most likely within a beamwidth of the declination of observation, $82^\circ\!.00 \pm 0^\circ\!.25$. Each of these sources has a signal which is stationary with respect to the sky (as determined by the various levels of chopping built into our observation strategy) and is detected in multiple channels. The compactness of these sources makes it implausible that they are due to diffraction or side-lobe effects.

We cannot rule out the possibility that these are are Galactic bremsstrahlung sources; observations at lower frequency ($\lesssim 3$ cm^{-1}) will shed light on this question. It would be somewhat unexpected for CMBR fluctuations obeying Gaussian statistics to produce such features, and we have performed simulations that indicate that these features are not consistent with the correlation functions considered here. For the detailed discussion in this paper, we have made the assumption that these are indeed unresolved foreground sources. The regions which are contaminated by these sources have been removed from consideration pending further analysis. In particular, only the region $15^{\rm h}\!.69 < {\rm RA} < 18^{\rm h}\!.55$ is included in the main CMBR results, though we also include results based the entire data set. A future *Letter* will address the detailed spectra and possible identification of these sources.

4.3. Limits on CMBR Anisotropy

To set limits on the anisotropy of the CMBR, we model the anisotropy $\Delta T(\mathbf{x})$ as a Gaussian random field described by a correlation function $C(|\mathbf{x}_1 - \mathbf{x}_2|) = \langle \Delta T(\mathbf{x}_1)\, \Delta T(\mathbf{x}_2)\rangle$. Our observations have been binned by orientation of the antenna pattern; call the antenna pattern as oriented for the kth observation $H_k(\mathbf{x})$. (Clearly all the functions H_k are translations and rotations of one function H.) Then the signal s_k from CMBR is $s_k = \int d\mathbf{x}\, H_k(\mathbf{x})\Delta T(\mathbf{x})$, and consequently the covariance of the s_k is

$$\langle s_k s_l \rangle = \int d\mathbf{x}_1\, d\mathbf{x}_2\, H_k(\mathbf{x}_1) H_l(\mathbf{x}_2) C(|\mathbf{x}_1 - \mathbf{x}_2|). \qquad (2)$$

To this signal our instrument adds noise n_k, which has the covariance $\langle n_k n_l \rangle = \delta_{kl}\sigma_k^2$. The instrument noise and sky signal are uncorrelated with each other, so the covariance of our observations $t_k \equiv s_k + n_k$ is just the sum of the covariances of s_k and n_k.

We set limits on the overall amplitude of the correlation function C by using the likelihood ratio statistic (Martin 1971). Let $(W_{kl})^{-1} = \langle s_k s_l \rangle + \sigma_k^2 \delta_{kl}$, and $(W^0_{kl})^{-1} = \sigma_k^2 \delta_{kl}$; then the likelihood ratio λ is

$$\lambda = \left(\frac{\det W}{\det W^0} \right)^{1/2} \exp \left(-\frac{1}{2} \sum_{kl} t_k (W_{kl} - W^0_{kl}) t_l \right) . \quad (3)$$

Let $\rho_C(\lambda)$ be the probability density function of λ under the hypothesis that the fluctuations obey the correlation function C, and let λ^* be the value of the statistic for our observations. Note that λ, λ^*, and ρ_C all depend on the correlation function, and in particular on its amplitude. Then the 95% confidence level upper limit on the amplitude is that amplitude for which the cumulative distribution function is

$$\int_0^{\lambda^*} d\lambda \, \rho_C(\lambda) = 0.95. \quad (4)$$

Similarly, the 95% lower limit is that amplitude for which this integral is 0.05, if such an amplitude exists. Taken together, these two limits form a 90% confidence interval. We perform the integral in (4) by Monte-Carlo integration (Press *et al.* 1986). The amplitudes we quote here are total rms fluctuation, i.e., $[C(0)]^{1/2}$.

Fig. 3 shows the upper and lower limits for total rms anisotropy as a function of correlation angle and assuming a Gaussian-shaped correlation function. This uses only the data in the region $15^{\rm h}.69 < {\rm RA} < 18^{\rm h}.55$. The single difference data is most sensitive at $\theta_c = 0^\circ.5$ with a 90% confidence interval of $0.6 \times 10^{-5} < \Delta T/T < 2.2 \times 10^{-5}$. For the double difference data, the most sensitive result is at $\theta_c = 0^\circ.3$, where $1.1 \times 10^{-5} < \Delta T/T < 3.1 \times 10^{-5}$. We have analyzed various subsets of the data, dividing the flight into unequal quarters. The first quarter is the region near MSAM 15+82, the second the following data up to the point where we moved off to observe the Coma cluster, the third the source-free data after the break, and the fourth the data near MSAM 19+82. Table 1 gives the upper and lower limits for each quarter of the flight as well quarters 2 and 3 on which these results are based. We emphasize that our observation strategy allows for independent measurements using the single and double difference demodulations.

5. Conclusions

The results from both the single and double difference data for this flight (declination 82° and $15^{\rm h}.69 < {\rm RA} < 18^{\rm h}.55$) show positive detections of sky brightness variations which are consistent with a CMBR spectrum. The placement of our spectral passbands allows for strong discrimination of warm Galactic dust from CMBR fluctuations, but some cold dust models at low levels are difficult to rule out. We cannot strongly rule out the spectrum of bremsstrahlung, though it is highly unlikely that that could cause a signal of the measured amplitude. Meinhold *et al.* 1993 have previously reported an upper limit ($\Delta T/T < 2.5 \times 10^{-5}$) at this angular scale.

The presence of the two unresolved sources in the data is clearly very interesting, and could imply a significantly different scenario for CMBR anisotropy measurements on $0^{\circ}.5$ angular scales at the $\Delta T/T \sim 1 \times 10^{-5}$ level. If the extrapolations of Franceschini *et al.* 1989 are correct, then it is not likely that this detection is due to unresolved extragalactic sources. However, the two sources in these data may indicate that there is a previously unsuspected population for which neither the spatial distribution nor the spectral signature is well determined by existing data. Alternatively, if these sources are true CMBR fluctuations, then we need to investigate the compatibility of these highly peaked features with various models. Clearly, a more complete understanding of these sources is central to further improvements in sensitivity to CMBR anisotropies.

Files containing the data on which Fig. 2 is based along with the antenna pattern will be made available. For information on how to obtain these data, fetch the file `/pub/data/msam-jun92/README` by anonymous FTP from `cobi.gsfc.nasa.gov`.

We would like to thank the staff of the National Scientific Balloon Facility in Palestine, Texas, who valiantly maintain the original can-do spirit of NASA. W. Folz provided electronics support and accompanied us on our observing run in Palestine. We would like to thank C. Lisse, J. Mather, H. Moseley, and R. Weiss for helpful discussions. The NSF Research and NASA Science Internet, which we take for granted too often, makes our long-distance collaboration possible without exorbitant expenditure of travel funds. This work made extensive use of the fine products of the Free Software Foundation of Cambridge, MA. The National Aeronautics and Space Administration supports this research through grants NAGW 1841, RTOP 188-44, NGT 50908, and NGT 50720. Lyman Page is supported by a grant from the National Science Foundation.

	θ_c	Quarter	RA (h)	Upper bound (μK)	Lower bound (μK)
Single difference	$0\overset{\circ}{.}5$	1	14.44–15.69	221	39
		2	15.69–16.89	99	—
		3	17.18–18.55	102	15
		4	18.55–20.33	221	62
		2+3	15.69–18.55	61	16
		All	14.44–20.33	116	53
Double difference	$0\overset{\circ}{.}3$	1	14.44–15.69	336	91
		2	15.69–16.89	139	33
		3	17.18–18.55	127	21
		4	18.55–20.33	121	37
		2+3	15.69–18.55	85	30
		All	14.44–20.33	97	50

Table 1: Upper and lower bounds on CMBR anisotropy

REFERENCES

Charakhch'yan, A. N., Bazilevskaya, G. A., Stozhkov, Yu. I., and Charakhch'yan, T. N. 1978, in *Cosmic Rays in the Stratosphere and in Near Space*, Proceedings of the P. N. Lebedev Physics Inst., Vol. 88 (New York: Consultants Bureau)

Efstathiou, G., Bond, J. R., and White, S. D. M. 1992, MNRAS, 258, 1

Franceschini, A., Toffolatti, L., Danese, L., and De Zotti, G. 1989, ApJ, 344, 35

Gorski, K. 1993, ApJ, in press

Griffin, M. J. *et al.* 1986, Icarus, 65, 244

Hanel, R. A. *et al.* 1981, Journal of Geophysical Research, 86, 8705

Harwit, M. 1988, Astrophysical Concepts, 2nd Ed., (New York: Springer-Verlag)

Kashlinsky, A. 1992 ApJ, 387, L1

Lang, K. R. 1980, Astrophysical Formulae, 2nd Ed., (New York: Springer-Verlag)

Martin, B. R. 1971, Statistics for Physicists (London: Academic)

Meinhold, P. *et al.* 1993, ApJ, 409, L1

Meyer, S. S., Cheng, E. S., and Page, L. A. 1991, ApJ, 371, L7

Page, L. A. 1989, Ph.D. thesis, MIT

Page, L. A., Cheng, E. S., and Meyer, S. S. 1990, ApJ, 355, L1

Page, L. A., Cheng, E. S., Golubovic, B., Gundersen, J., and Meyer, S. M. 1993, Appl.Optics, in press

Press, W. H. *et al.* 1986, Numerical Recipes: The Art of Scientific Computing (Cambridge: Cambridge Univ.)

Smoot, G. F. *et al.* 1992, ApJ, 396, L1

Wheelock, S. *et al.* 1991, IRAS Sky Survey Atlas, $|\beta| > 50$ degrees, Explanatory Booklet, (Pasadena:JPL)

Wheelock, S. *et al.* 1993, Explanatory Supplement to the IRAS Sky Survey Atlas (Pasadena:JPL) in press

This manuscript was prepared with the AAS LaTeX macros v3.0.

Figure 1. Optical depth at 22.5 cm^{-1} of dust component D_k; a) Double difference demodulation, b) Single difference. Superimposed curve is *IRAS* 100 μm data convolved with our antenna pattern; scale is set by fit to our observations.

Figure 2. CMBR component t_k; a) Double difference, b) Single difference. Antenna pattern is superimposed for reference.

Figure 3. Upper and lower limits on CMBR anisotropy for Gaussian-shaped power spectra with correlation length θ_c, based on data between right ascensions $15\overset{h}{.}69$–$18\overset{h}{.}55$. 95% CL upper limit for double difference (solid) and single difference (long dashed); 95% CL lower limit for double difference (dashed) and single difference (dotted).

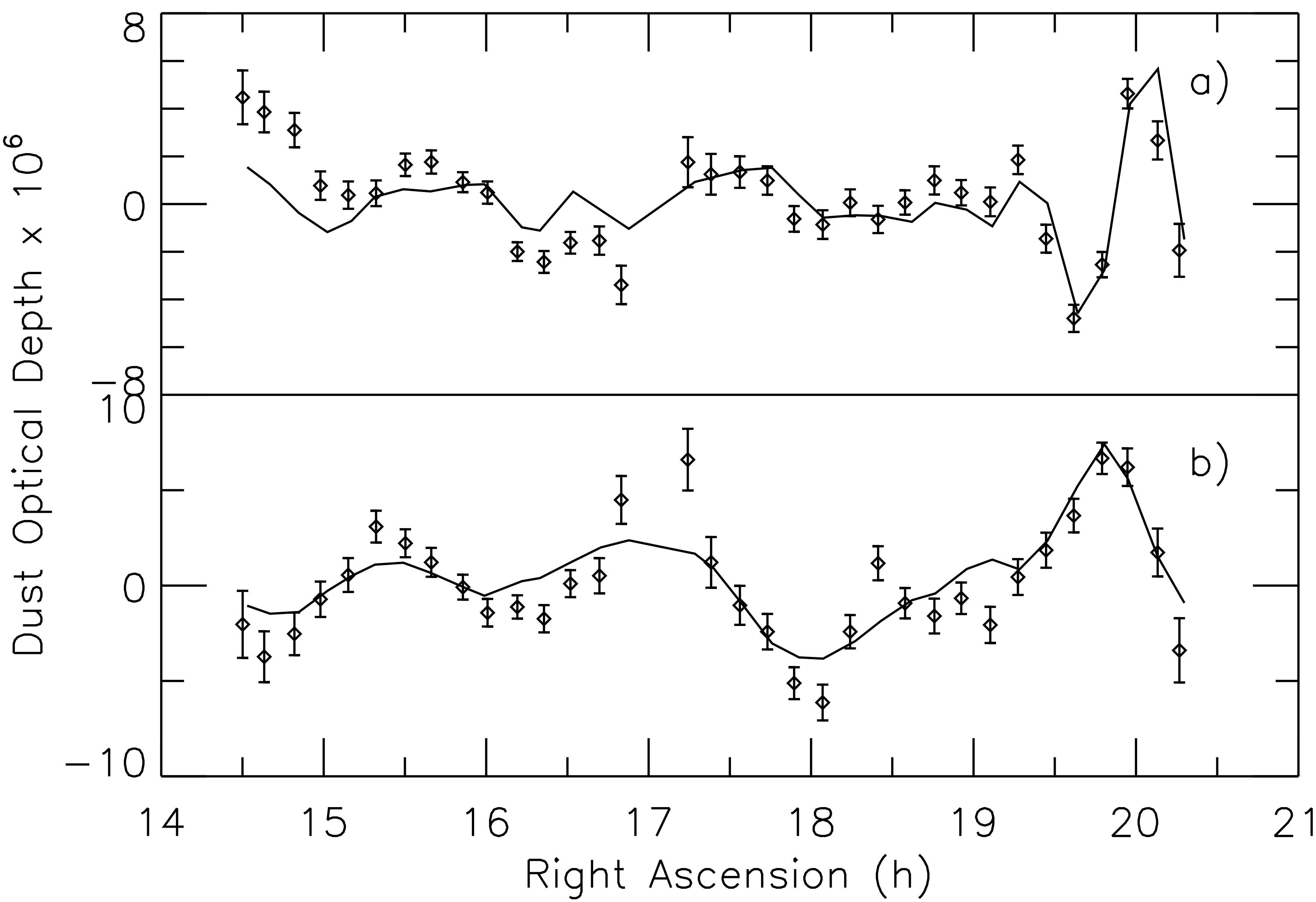

Dust Optical Depth x 10^6
8
0
−8
10
0
−10
a)
b)
14
15
16
17
18
19
20
21
Right Ascension (h)

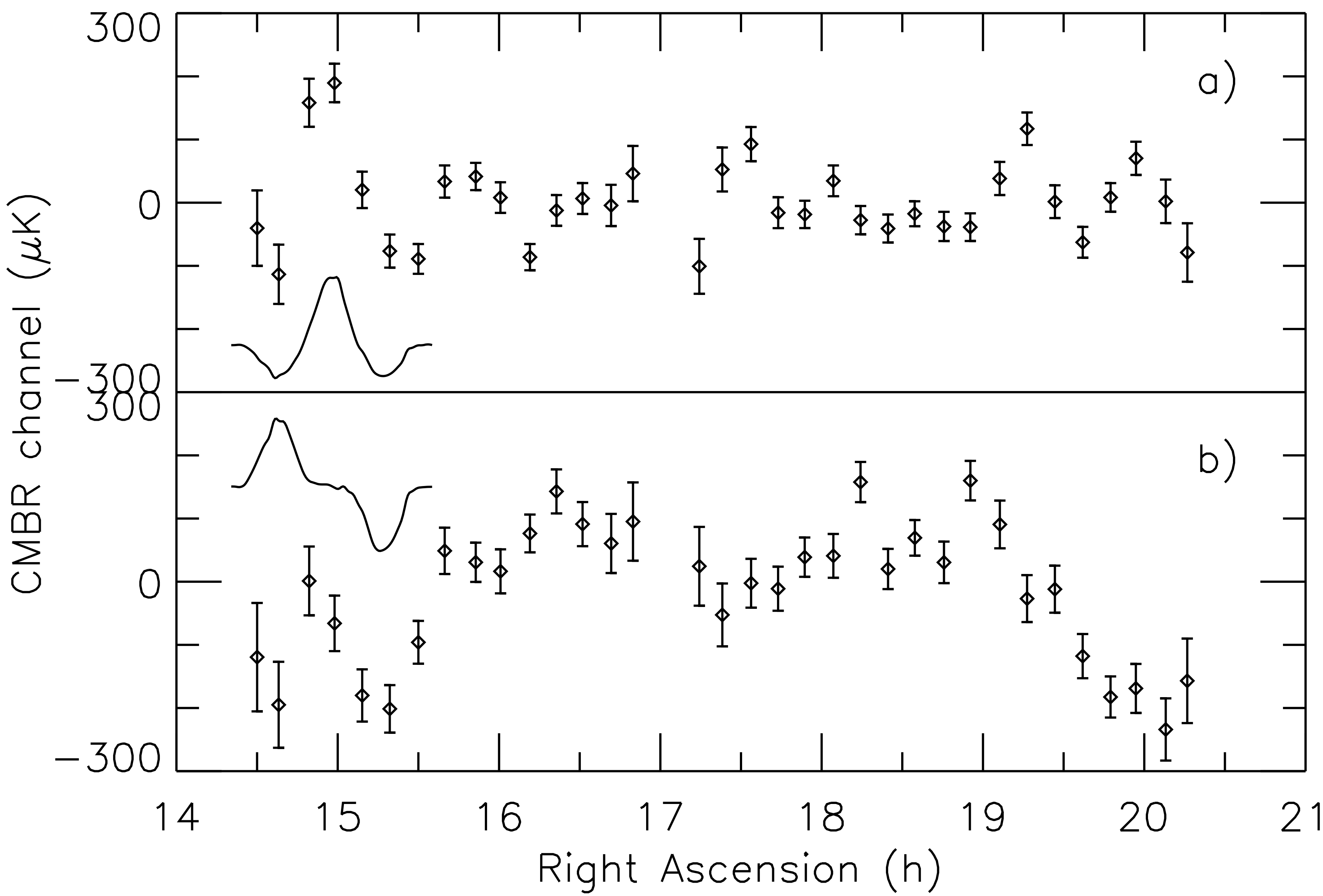

CMBR channel (μK)
300
0
−300
a)
b)
14
15
16
17
18
19
20
21
Right Ascension (h)

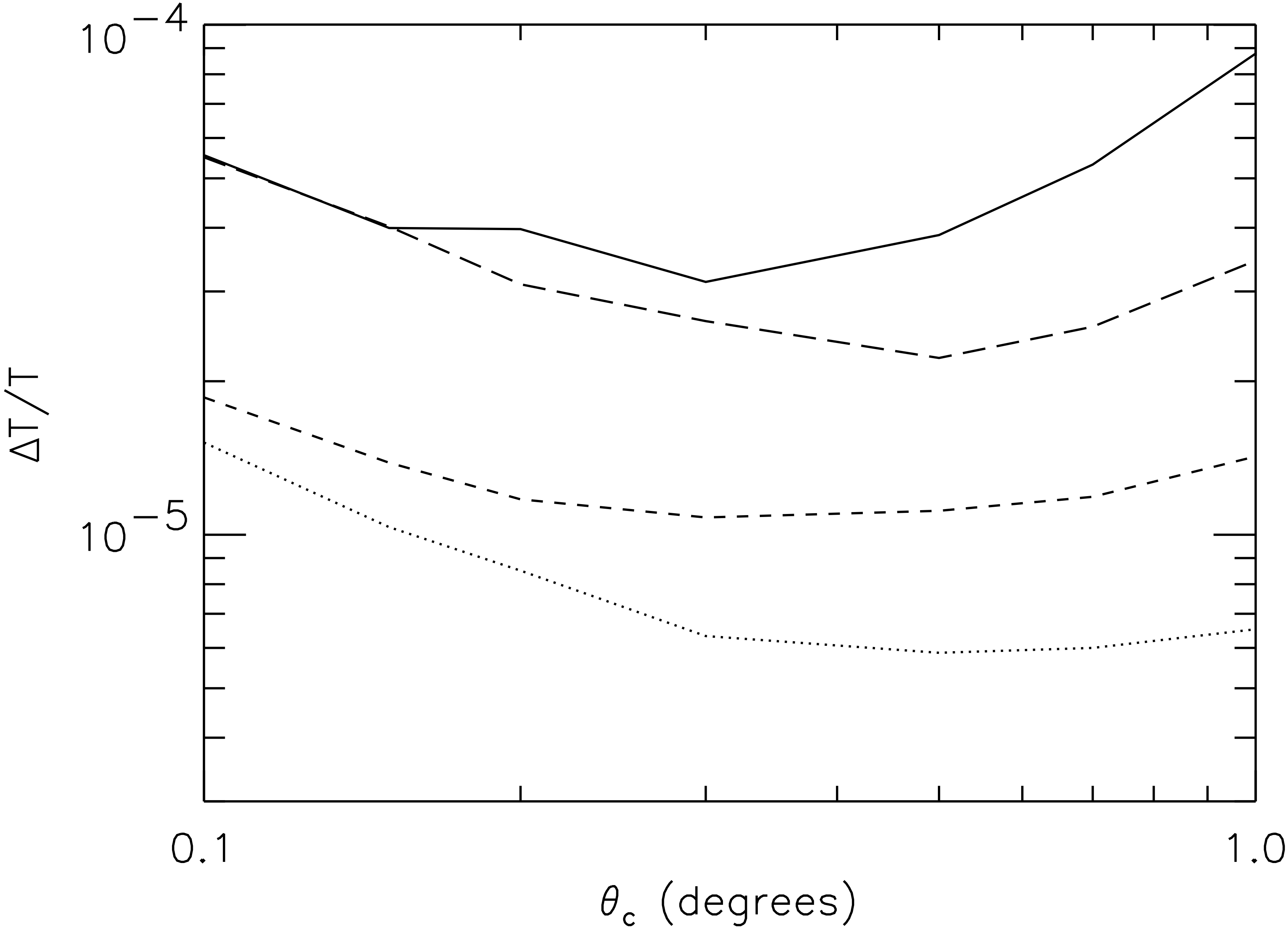

10−4
10−5
ΔT/T
0.1
1.0
θc (degrees)